Making Contacts to n-Type Organic Transistors Using Carbon Nanotube Arrays

Fabio Cicoira,[†,§] Carla M. Aguirre,[‡] and Richard Martel[§,*]

[†]Istituto di Fotonica e Nanotecnologie, Consiglio Nazionale delle Ricerche, Via alla Cascata 56/c, Trento 38123, Italy, [‡]Département de Genie Physique, École Polytechnique de Montréal, Montréal, Québec H3C 3A7, Canada, and [§]Département de Chimie, Université de Montréal, Montréal, Québec H3C 3J7, Canada

ABSTRACT We investigated the performance of carbon nanotube (CNT) array electrodes applied to n-type and ambipolar phenyl-C61-butyric acid methyl ester (PCBM) thin film transistors on a SiO_2 dielectric substrate. Compared to conventional Au electrodes, CNT arrays provide better injection efficiency, improved switching behavior, higher electron mobility, and lower contact resistance. Experiments on ambipolar PCBM transistors indicate that the injection performance is enhanced by the electrostatics of the CNT contacts, which promotes electron and hole tunneling across Schottky barriers at the PCBM/nanotube interface. The use of CNT arrays is a valid replacement to low workfunction metals, which are often reactive in air and difficult to process. Our work paves the way for a widespread use of carbon nanotube array electrodes in high-performance n-type and p-type organic thin film transistors.

KEYWORDS: organic transistors · charge carrier injection · ambipolar transport · carbon nanotubes · Schottky barriers · contacts

The performance of organic thin film transistors (OTFTs) has improved considerably over the last decades owing to important progress in organic semiconductor synthesis and device engineering.[1−4] The electrical characteristics of OTFTs are, however, limited by the contacts, whose resistance depends critically on the electrostatics and on the local details of the electrodes/organic semiconductor interface.[5−8] For instance, charge carrier injection efficiency can be limited by the presence of Schottky barriers that originate from an offset between the metal workfunction and the highest occupied molecular orbital (HOMO, for hole injection) or the lowest unoccupied molecular orbital (LUMO, for electron injection) of the organic semiconductor,[9,10] or to additional offsets induced by local charge transfer to acceptor/donor states. The presence of impurities, morphological discontinuities, interfacial traps, and structural disorder in the organic film at the electrode interface are other factors affecting the energy level alignment and the charge carrier injection properties.[11−13] Low injection efficiency has been so far a severe performance hurdle for bottom contact OTFTs (with bottom gate), that is, the most interesting geometry for organic microelectronics. Although progress has been achieved using thiol self-assembled monolayers,[14−17] a universal approach to optimize the charge injection efficiency in OTFTs remains to be developed.

The use of carbon nanotubes (CNTs) to optimize charge carrier injection in OTFTs is attractive because their one-dimensional (1D) structure can induce strong electrostatic effects at the electrode/semiconductor interface. One-dimensional electrostatic effects around CNTs were clearly identified in carbon nanotube field-effect transistors and shown to promote charge carrier tunneling across the contact Schottky barriers.[18−22] Other advantages for the use of CNTs are high electrical conductivity, ease of processing, compatibility with flexible electronics, and chemical inertness.[23] CNT electrodes have already been used in organic electronic devices. Hole injection has been demonstrated in organic light emitting diodes (OLEDs) and in p-type OTFTs.[24−28] Recently, OLEDs having CNT layers as anode and cathode have been reported.[29]

In this work, we investigated the performance of CNT arrays as source/drain electrodes for n-type phenyl-C61-butyric acid methyl ester (PCBM) OTFTs on a SiO_2/Si substrate. As shown in Figure 1a, the CNT electrodes consist of a disordered array of individual (or small bundle of) nanotubes having one end connected to a large metal (Ti) pad and the other end embedded in the organic semiconductor layer. This electrode geometry preserves the 1D structure of the nanotubes and aims to provide optimum conditions enabling 1D electrostatics. Compared to conventional Au source/drain

*Address correspondence to r.martel@umontreal.ca.

Received for review October 9, 2010 and accepted November 23, 2010.

Published online December 9, 2010. 10.1021/nn1027032

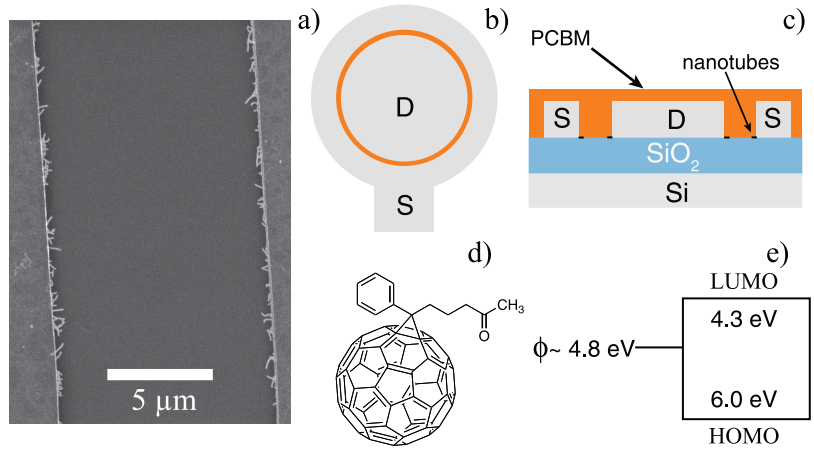

Figure 1. Scanning electron microscopy image (1 KeV, 7 μA) of single-wall CNT array electrodes (a); top view (b) and cross section (c) scheme of concentric source (S) and drain (D); molecular structure of PCBM (d); energy band diagram of PCBM with respect to a workfunction of 4.8 eV (close to that of CNTs).[38] For PCBM, we used a LUMO energy of 4.3 eV, which is on the high end of the values reported by the literature, *i.e.*, −3.7 to −4.3 eV,[39] and a HOMO energy of 6.0 eV (e).[40]

electrodes, CNT arrays provide better electron injection efficiency, improved switching behavior, higher electron mobility, and lower contact resistance. After vacuum annealing, the n-type PCBM OTFTs were converted to ambipolar and used to investigate electrostatic effects induced by the arrays at the CNT/PCBM interface. Our experiments support the main hypothesis that 1D electrostatic effects can be used to enhance charge carrier injection in organic semiconductors and demonstrate that carbon nanotube arrays are a viable contact scheme for making higher performance organic field-effect transistors.

RESULTS AND DISCUSSION

We fabricated bottom contact (bottom gate) OTFTs having source (S) and drain (D) electrodes made of arrays of individual (or small bundle of) single-wall CNTs (the so-called *hairy electrodes*).[24] The CNTs (few micrometers in length) were attached to the SiO_2 surface by the means of concentric Ti (S/D) contact pads. The CNT length from the metal contact edge was roughly 200 nm (Figure 1a). The concentric electrode geometry (Figure 1b,c) is the most suitable to evaluate the electrode injection performance because it allows to circumvent parasitic currents.[30,31] As an organic semiconductor, we selected PCBM (Figure 1d), which is a benchmark material for n-type OTFTs,[32−36] and it is widely employed as an electron acceptor in organic photovoltaic cells.[37]

The output characteristics, taken without thermal annealing, in vacuum (10^{-7} Torr), at 300 K of PCBM OTFTs employing CNT array electrodes (hereafter referred to as CNT OTFTs, Figure 2a) and benchmark Au electrodes (Au OTFTs, Figure 2c) show unipolar n-type transistor behavior. The comparison highlights the superior performance of the CNT over Au electrodes. As emphasized by the output characteristics at low drain voltage (V_d) (Figure 2b,d), CNT OTFTs show linear drain current−drain voltage (I_d−V_d) characteristics and good injection efficiency. On the contrary, Au OTFTs show a sublinear behavior, which indicates that electron injection is strongly limited by the presence of an injection barrier. CNT OTFTs also show higher saturation I_d and electron mobility (μ_e). For the device characteristics reported in Figure 2, in the saturation regime (gate voltage, $V_g = 20$ V), we extracted $\mu_e \approx 2 \times 10^{-2}$ cm^2 V^{-1} s^{-1} for CNT OTFTs (turn-on voltage, $V_{ON} \approx 4.5$ V; threshold voltage, $V_T \approx 6$ V; and on/off ratio, $I_{ON}/I_{OFF} \approx 10^6$) and $\mu_e \approx 1 \times 10^{-3}$ cm^2 V^{-1} s^{-1} for Au OTFT ($V_{ON} \approx 5$ V; $V_T \approx 10$ V; and $I_{ON}/I_{OFF} \approx 10^5$). At higher V_g (*e.g.*, $V_g = 40$ V), we typically find $\mu_e \approx 1.0 \times 10^{-2}$ (±10%) cm^2 V^{-1} s^{-1} for CNT OTFTs and $\mu_e \approx 6.0 \times 10^{-3}$ (±30%) cm^2 V^{-1} s^{-1} for Au OTFTs (see Figure S1 in Supporting Information, and Figure 5b,d). Thus, the difference between the μ_e of CNT and Au OTFTs decreases with V_g, which indicates that the CNT contact scheme provides significantly better performance at low gate field (voltage). The same behavior is observed with the drain voltage (Figure S2 in Supporting Information): in the linear regime ($V_d = 2$ V), μ_e for CNT OTFTs is about 2 orders of magnitude larger than μ_e for Au OTFTs, whereas in the saturation regime ($V_d = 20$ V), μ_e for CNT OTFTs and for Au OTFTs has similar values. The differences in mobility are therefore the most significant at small drain and gate fields, which are conditions where contact barriers, instead of channel resistance, dominate the total resistance of the devices. It is worth noticing that the μ_e of our devices, obtained without any treatment of the SiO_2 surface, is similar to that of state-of-the-art bottom contact PCBM OTFTs.[32] Moreover, the Arrhenius plots of μ_e for CNT and Au OTFTs (Figure S2 in Supporting Information) indicate that the electron transport is thermally activated, which is expected for disordered organic semiconductors.[41] Last, Ti electrodes with no CNT lead to extremely poor OTFT performance (Figure S3 in Supporting Information), which proves that the large majority of the electrons in CNT OTFTs are indeed injected from the nanotube arrays.

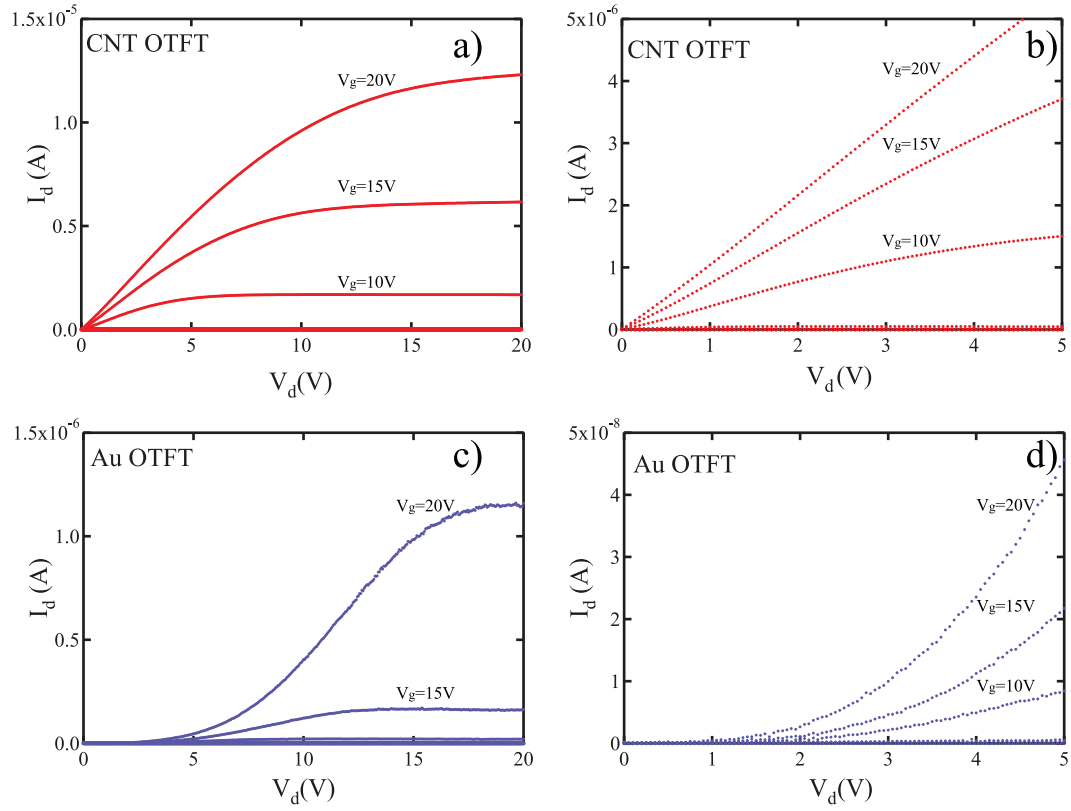

Figure 2. Output characteristics (I_d *versus* V_d at various V_g) at 300 K of PCBM OTFTs with CNT (a) and Au (c) S/D electrodes for V_g = 0, 5, 10, 15, 20 V (the highest currents being measured at V_g = 20 V). Output characteristics for 0 < V_d < 5 of the same devices with CNT (b) and Au (d) electrodes. V_d has +50 mV steps (W/L = 2000/10 μm/μm).

The contact resistance (R_c) of the CNT OTFT devices was extracted from the device resistance (R_{on}) calculated for variable channel length (L), owing to the linear I_d-V_d relationship at low V_d (Figure 3).[7,9,42] Extrapolation at L = 0 of R_{on} at V_g = 15 V and V_g = 20 V (for 0 V < V_d < 3 V) gives a R_c of ≈200 kΩ (the normalized contact resistance, $R_cW \approx$ 50 kΩ cm). For Au OTFTs, R_c could not be extracted due to the nonlinear I_d-V_d relationship at low V_d.[43] However, literature data (at similar V_g) for R_c of bottom contact PCBM OTFTs with Au electrodes (with similar channel width, W) are in the tens of MΩ range,[44] which again indicates a substantially lower value for our CNT OTFT. The R_c here measured with our CNT OTFTs is overall low for bottom contact devices, although lower values with metal electrodes have been previously obtained.[45,46]

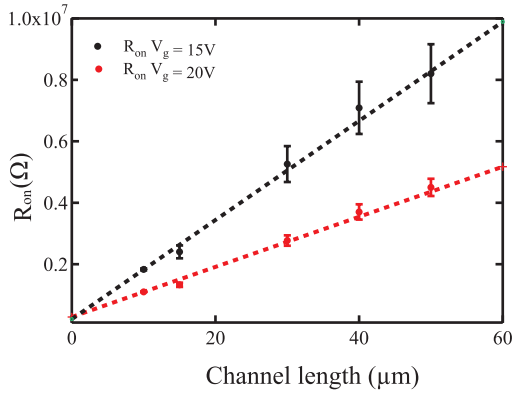

Figure 3. Channel resistance (R_{on}) *vs* channel length (L) for CNT OTFTs (0 V < V_d < 3 V, W = 2000 μm, and L = 10, 15, 30, 40, and 50 μm). The extrapolation of R_{on} at L = 0 gives the contact resistance R_c.

The transfer characteristics in the linear and saturation regimes (Figure 4a–d) demonstrate the superior performance of CNT over Au OTFTs, that is, a higher I_{ON}/I_{OFF}, a lower V_T and a steeper subthreshold swing (SS = $dV_g/d\log_{10}I_d$). The most striking differences are found in the linear regime at V_d = 2 V, where I_d is more than 2 orders of magnitude higher for CNT OTFTs (Figure 4a,c). Moreover, in the subthreshold region, I_d increases exponentially with V_g for CNT OTFTs whereas it increases more gradually for Au OTFTs. For CNT OTFTs, SS is typically about 400 mV/decade,[47] which is small for OTFT but large compared to SS of state-of-the-art metal-oxide-semiconductor field-effect transistors (MOSFETs) having no Schottky barrier (SS = 60 mV/decade at room temperature).[48] Moreover, SS for CNT OTFTs does not show clear temperature (T) dependence between 200 and 380 K (Figure S4 in Supporting Information), whereas SS is proportional to T for silicon MOSFETs.[48] Assuming a low density of interfacial traps, the larger than expected SS and the absence of T dependency are signatures of contact switching and of the presence of a Schottky barrier at the contacts.[19] These results also suggest that the injection involves tunneling across a contact barrier.

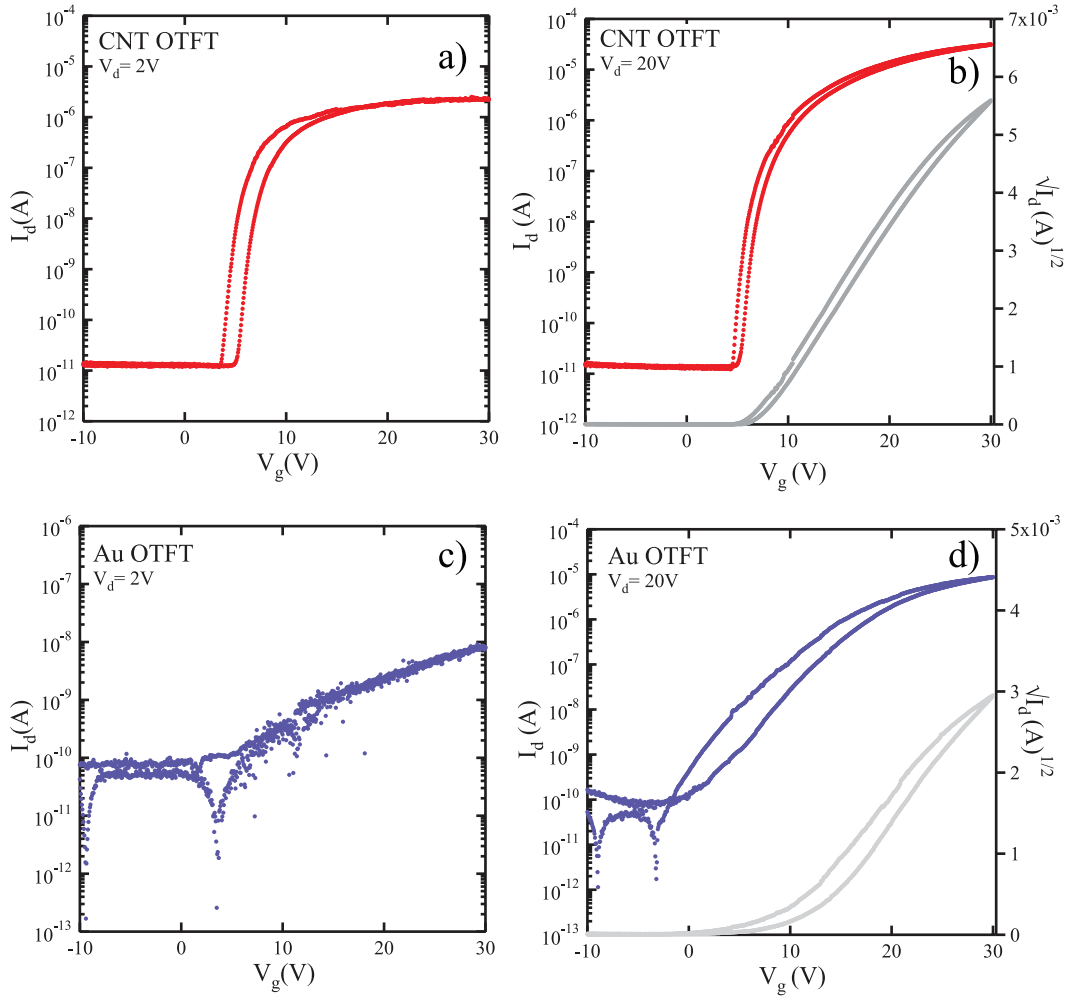

Figure 4. Transfer characteristics (I_d *versus* V_g) in the linear regime (V_d = 2 V) at 300 K of PCBM OTFT with CNT array (a) and Au (c) electrodes in semilog plot; transfer characteristics in the saturation regime (V_d = 20 V) at 300 K of PCBM OTFT with CNTs (b) and Au (d) in semilog and linear plots. V_g has 100 mV steps (W/L = 2000/10 μm/μm).

Compared to the Au, CNT OTFTs present smaller I_d hysteresis between the forward and reverse V_g sweeps (Figure 4b,d). The hysteresis is typically attributed to trapping/detrapping of charge carriers.[49,50] As the devices studied here present similar PCBM/oxide interfaces and only differ by their injecting electrodes, this result points to a lower concentration of interfacial traps at the CNT/PCBM interface.[24,51] Overall, all of our experimental results prove that CNT array electrodes provide better performance than Au electrodes, especially at low bias. Thus, we conclude that the CNT arrays improve the injection as well as the overall performance of n-type OTFTs.

To further explore the performance enhancement induced by the CNT contacts, the unipolar n-type PCBM OTFTs were converted to ambipolar OTFTs by vacuum (10^{-7} Torr) annealing at 400 K for 16 h. The yield of conversion for more than 10 devices is close to 100%. The conversion from unipolar n-type to ambipolar transport is shown in the output (Figure 5a−d) and in the transfer characteristics (Figure 6) for both CNT and Au OTFTs (after annealing, we extracted $\mu_h \approx 10^{-4}-10^{-5}$ $cm^2\ V^{-1}\ s^{-1}$, whereas no significant hole transport had been measured before annealing). The same conversion has been previously observed in bottom contact PCBM OTFTs employing a HMDS passivated SiO_2 dielectric and Au electrodes.[32] On a bare SiO_2 dielectric, unipolar to ambipolar conversion upon vacuum annealing has been observed for a few organic transistors[40,52] and for CNT (not organic) transistors.[22,53] Recent experiments on CNT transistors have shown that the conversion to ambipolar transport is due to the desorption of O_2 and H_2O molecules (*i.e.*, the oxygen−water redox couple) adsorbed at the surface of the SiO_2.[54] Because of the similarities between these works and our experiments on OTFTs, we ascribed the conversion to a similar charge transfer mechanism that involves molecular traps and Fermi level pinning at the SiO_2 surface.

The better performance of the CNT OTFTs over Au OTFTs can be qualitatively understood by analyzing the characteristics of the devices in relation with the different electrode/organic interfaces. Because the CNT arrays are composed of isolated CNTs embedded into the organic films (Figure 1), the electrodes induce a

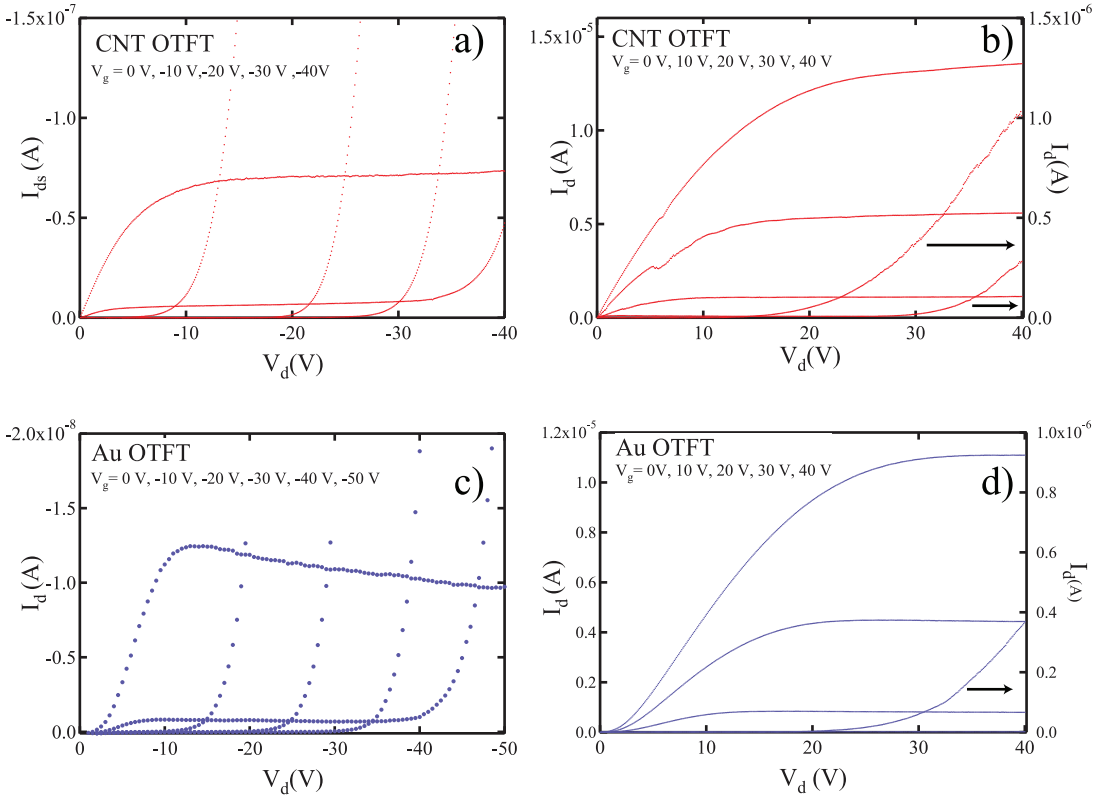

Figure 5. Images of p-type (a,c) and n-type (b,d) output characteristics for CNT OTFT and Au OTFT after vacuum annealing (16 h at 400 K). $|V_d|$ steps are 100 mV in panels a, b, and d and 500 mV in panel c. The curves at $V_g = 0$ V and $V_g = 10$ V in panel b and $V_g = 0$ V in panel d are shown in the magnified right *y* scales. Note that $V_g = 0, 10, 20, 30, 40$ V in panels a, b, and d and that $V_g = 0, 10, 20, 30, 40, 50$ V in panel c ($W/L = 2000/30$ μm/μm).

minimum perturbation to the organic layer.[24] Thus, it is expected that the CNT contact scheme, compared to Au, provides better structural ordering of organic layers and lower impurity and trap densities. This is consistent with the smaller hysteresis and SS found in the characteristics of the CNT OTFTs (Figure 4). However, structural defects and traps can only add series resistance (and hysteresis) to the device characteristics, which cannot explain the electric field dependence of the I_d-V_d. Therefore, a complete picture of the situation can only be drawn if additional contributions from the

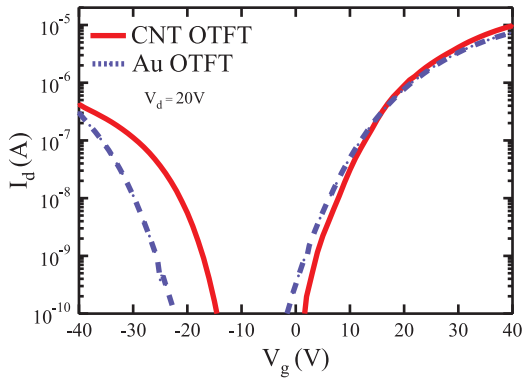

Figure 6. Ambipolar transfer characteristics at $V_d = 20$ V of CNT (red markers, full line) and Au (blue markers, dashed line) OTFTs (c) after vacuum annealing (16 h at 400 K). $|V_g|$ steps are 1000 mV ($W/L = 2000/30$ μm/μm).

device Schottky barriers at the PCBM/electrode interface are included in the discussion.

Past works on silicon MOSFETs have extensively covered the topic of Schottky barrier transistors, and this knowledge is useful in order to identify specific signatures of Schottky barriers to the OTFT characteristics.[55] The main evidence is the nonlinear I_d-V_d at low V_d and current leakage in the subthreshold region, which are both clearly seen in our Au OTFT characteristics (Figures 2c,d and 5c,d). Surprisingly, the I_d-V_d characteristics of the CNT OTFTs (Figure 2a,b), including the ambipolar devices (Figure 5a,b), are all linear (ohmic) in the ON state, even at very low V_d. This feature rather suggests that the CNT electrodes present no Schottky barrier. This assumption, which might be realistic only in the presence of a strong pinning of the Fermi level on the LUMO, can however be ruled out in our case for the following reason. For ambipolar OTFTs, because of the PCBM band gap, a Fermi level pinning on the LUMO level would indeed decrease the barrier for electron injection but, at the same time, increase the barrier for hole injection. The I_d-V_d characteristics of the ambipolar CNT OTFTs are ohmic for both hole and electron branches (Figure 5a,b), which indicates that the barriers are transparent electrically. We believe this point is key to understanding the exceptional performance observed with CNT array electrodes.

It is reasonable to expect large Schottky barriers between both the Au and CNT electrodes and the PCBM layer. One can roughly estimate the barrier heights using available literature data as follows: Assuming an unpinned Fermi level (*i.e.*, low density of interface states), the Fermi level of single-walled CNT contacts (workfunction is about 4.8 eV)[38] is offset by at least ~0.5 eV with respect to the LUMO (*i.e.*, between 3.7 and 4.3 eV relative to the vacuum level)[39] and by ~1.2 eV with respect to the HOMO (*i.e.*, 6.0 eV relative to the vacuum level)[40] of PCBM (see Figure 1e). The workfunction of evaporated Au lies between 4.4 and 4.6 eV, which should lead to similar offsets.[56] With these estimates in hand, it is interesting to note that the electron currents of both CNT and Au OTFTs at high $|V_g|$ are more than 1 order of magnitude larger than the hole currents (see ambipolar devices in Figure 6), thereby supporting a lower barrier height for electron injection (assuming similar mobility for electrons and holes). This is consistent with the estimates of about the position of the energy levels, which gives asymmetrical barriers to the PCBM LUMO and HOMO levels (see Figure 1e).

There are indirect evidences in the comparison between CNT and Au OTFTs that support our hypothesis of 1D electrostatic effects with the CNT array electrodes. As mentioned above, the CNT arrays (Figure 1a) present individual CNTs having a form factor that favors 1D electrostatics. In contrast, the Au contacts are better described using bidimensional (2D) electrostatics. The latter case, that is, a metal electrode in contact with a semiconductor, has been extensively studied in the context of regular MOSFETs.[57] In the presence of large Schottky barriers (*i.e.*, larger than $kT \approx 0.026$ eV), the 2D electrostatic effects have little influence on the length scale of the band bending (more precisely here the energy level shift for the organic materials) at the contacts. The length scale in 2D is mainly set by the gate oxide thickness (here $t_{ox} \sim 100$ nm), and the depletion zone is generally large in width. As a result, tunneling injection across the Schottky barrier is suppressed at low field.[48] The absence of tunneling at low V_d induces nonlinear I_d-V_d, which is a typical signature of Schottky barriers in regular 2D MOSFET structures.[55] It is therefore not surprising that the characteristics observed for most bottom contact OTFTs, including our Au OTFTs (Figures 2c,d and 5c,d), are nonlinear. A different scenario is possible in the presence of 1D electrostatics because the 1D fields are strongly enhanced in the contact region. Experiments and theoretical simulations on CNT transistors have demonstrated that 1D Schottky barriers extend for only a few nanometers and result in short depletion zones for which strong tunneling injection is possible.[19−22] That is, even in the presence of large Schottky barriers, the I_d-V_d characteristics of 1D systems are linear at low V_d because of strong tunneling across the barrier. This signature is consistent with the characteristics observed in our CNT OTFTs. Although the details of the electrode−semiconductor interface are different in this comparison,[58] the results with CNT OTFTs contain good evidences of 1D electrostatic effects in the contact region. Obviously, further work will be required to evaluate quantitatively the impact of the nanotube geometry on carrier injection mechanism.

In summary, we have demonstrated that a better carrier injection in PCBM films is obtained with CNT array electrodes compared to Au electrodes. For n-type PCBM OTFTs, the CNT arrays display a close to ideal injection behavior, high FET mobility, low contact resistance, and good subthreshold characteristics. For ambipolar PCBM OTFTs, CNT electrodes also show improved injection performance for both types of carriers compared to Au electrodes. These results indicate that our OTFT function as *Schottky barrier transistors*.[19] The better carrier injection in CNT OTFTs is qualitatively explained by an enhancement of the tunneling across the Schottky barrier due to 1D electrostatics effects induced by the form factor of the CNTs. The exceptional injection efficiency of CNTs represents a novelty in organic electronics. CNT arrays are a valid replacement to low workfunction metals, which are often reactive in air and difficult to process. Our work paves the way for a widespread use of CNTs as electrodes in both p- and n-type OTFTs.

METHODS

Sample Preparation and Measurements. Bottom contact, bottom gate transistors were prepared on a highly doped (n-type) Si(100) wafer covered with a 100 nm thermally grown SiO_2 dielectric (32 nF cm^{-2} capacitance). Carbon nanotube hairy electrodes (Figure 1a) were fabricated using a subtractive patterning technique.[24] A dense network of individual or small bundle single-wall carbon nanotubes (SWCNTs) was deposited in three steps from a 2% sodium cholate dispersion of SWCNT (1×10^{-4} mg/mL) in water. The CNT solution was first vacuum filtered on an amino-cellulose filter and then transferred to a SiO_2 surface that was previously treated with hexamethyldisilazane (HMDS) to improve nanotube adhesion. The filter was last dissolved in acetone. Ti concentric source/drain contacts (20 nm thick) were patterned on top of SWCNTs by photolithography and lift off. The samples were then sonicated while immersed in a photoresist stripper (AZ300T, Clariant). This sonication removes the nanotubes not directly attached to the Ti contacts and cuts the remaining CNT to an average length of 200 nm, yielding hairy electrodes, as shown in Figure 1a. The substrates so obtained were annealed in vacuum at 800 K for 1 h to decrease the contact resistance between nanotubes and Ti. This annealing step also led to the desorption of HMDS deposited at the beginning of the processing, leaving a bare SiO_2 surface.[59] To benchmark our nanotube electrodes, we also fabricated Au electrodes (thickness 40 nm) with a Ti adhesion layer (thickness 4 nm) having identical concentric geometry. To facilitate the comparison with CNT electrodes, these substrates were also annealed in vacuum at about 800 K for 1 h. Devices with channel width, $W = 2000$ μm, and channel length, $L = 10$, 15, 30, 40, and 50 μm, were used.

Substrate Cleaning and PCBM Deposition. Prior to organic semiconductor deposition, substrates with CNT electrodes were cleaned by low power sonication in acetone and isopropyl alcohol. Au electrodes were cleaned by the same treatment followed by UV/ozone exposure.

Thin films of phenyl-C61-butyric acid methyl ester (PCBM, Kintec, Figure 1d) were deposited by spin coating (1000 rpm, 1 min) from a 9 mg/mL solution in anhydrous chlorobenzene (Aldrich) under N_2 atmosphere. The samples were briefly exposed to air before electrical measurements.

Electrical Measurements and Device Parameter Extraction. Electrical measurements were performed in the dark and under vacuum (10^{-7} Torr) using an Agilent (B1500A) semiconductor parameter analyzer and a Desert Cryogenic electrical probe station. To exclude the presence of CNTs between the S/D electrodes, substrate for CNT OTFTs were also measured before PCBM deposition.

The field-effect mobility, μ_e, at saturation was calculated according to the formula $I_d = (W/2L)\mu_e C_i(V_g - V_T)^2$, where I_d is the drain current at the saturation, V_g the gate voltage, W the channel width, L the channel length, C_i the capacitance per unit area of SiO_2 (32 nF cm^{-2}), and V_T the threshold voltage. V_T was determined from the transfer curve in the linear regime ($V_d = 2$ V) by extrapolating the intersection of I_d with the gate voltage (V_g) axis; μ_e in the linear regime was calculated from the transconductance, dI_d/dV_g, according to the formula $\mu_e = (dI_d/dV_g)(L/WC_iV_d)$, where V_d is the drain voltage. The turn-on voltage (V_{ON}) was determined as the V_g at which the current abruptly increases in the semilog plot of the transfer characteristics.

The contact resistance (R_c) was extracted extrapolating the device resistance (R_{on}) at $L = 0$ in plots of R_{on} *versus* channel length. R_{on} was determined as dV_d/dI_d from the linear region (0−3 V) of the I_d *versus* V_d plots of CNT OTFTs at $V_g = 15$ V and $V_g = 20$ V.

Scanning Electron Microscopy (SEM) Imaging. SEM images of the CNT hairy electrodes were acquired using a Hitachi field emission S-4700 microscope.

Acknowledgment. The authors are grateful to Clara Santato and Jill A. Miwa for fruitful discussions. The authors thank Dr. Benoit Simard's group from Steacie Institute at NRC for generous donation of the single-wall carbon nanotubes. F.C. acknowledges the Marie Curie Program of the European Commission (Grant MC-OIF-CT-2006-040864 TOPOS) for financial support. Part of this work was carried out at the Central Facilities of École Polytechnique and Université de Montréal. This project is supported by the Canada Research Chair (CRC) and NSERC Discovery grants.

Supporting Information Available: Electrical output characteristics of CNT OTFTs and Au OTFTs at high gate voltage; Arrhenius plot of the electron mobility for CNT OTFTs and Au OTFTs in linear ($V_d = 2$ V) and saturation ($V_d = 20$ V) regimes; electrical output characteristics of Ti-contacted PCBM OTFTs; transfer characteristics of CNT OTFTs and Au OTFTs at variable temperature. This material is available free of charge *via* the Internet at http://pubs.acs.org.

REFERENCES AND NOTES

1. Street, R. A. Thin-Film Transistors. *Adv. Mater.* **2009**, *21*, 2007–2022.
2. Malliaras, G. G.; Friend, R. H. An Organic Electronics Primer. *Phys. Today* **2005**, *58*, 53–58.
3. Dimitrakopulos, K.; Malenfant, P. R. L. Organic Thin Film Transistors for Large Area Electronics. *Adv. Mater.* **2002**, *14*, 99–117.
4. Zaumseil, J.; Sirringhaus, H. Electron and Ambipolar Transport in Organic Field-Effect Transistors. *Chem. Rev.* **2007**, *107*, 1296–1323.
5. Burgi, L.; Richards, T. J.; Friend, R. H.; Sirringhaus, H. Close Look at Charge Carrier Injection in Polymer Field Effect Transistors. *J. Appl. Phys.* **2003**, *94*, 6129–6137.
6. Braun, S.; Salaneck, W. R.; Fahlman, M. Energy-Level Alignment at Organic/Metal and Organic/Organic Interfaces. *Adv. Mater.* **2009**, *21*, 1–23.
7. Hamadani, B. H.; Natelson, D. Extracting Contact Effects in Organic FETs. *Proc. IEEE* **2005**, *93*, 1306–1311.
8. Kahn, A.; Koch, N.; Gao, W. Electronic Structure and Electrical Properties of Interfaces Between Metals and π-Conjugated Molecular Films. *J. Polym. Sci., Part B: Polym. Phys.* **2003**, *41*, 2529–2548.
9. Gundlach, D. J.; Zhou, L.; Nichols, J. A.; Jackson, T. N.; Necliudov, P. V.; Shur, M. S. An Experimental Study of Contact Effects in Organic Thin Film Transistors. *J. Appl. Phys.* **2006**, *10*, 024509.
10. Schroeder, R.; Majewski, L. A.; Grell, M. Improving Organic Transistor Performance with Schottky Contacts. *Appl. Phys. Lett.* **2004**, *84*, 1004–1006.
11. Tsuruma, Y.; Al-Mahboob, A.; Ikeda, S.; Sadowski, J. T.; Yoshikawa, G.; Fujikawa, Y.; Sakurai, T.; Saiki, K. Real-Time Observation and Control of Pentacene Film Growth on an Artificially Structured Substrate. *Adv. Mater.* **2009**, *21*, 4996–5000.
12. Tsen, A. W.; Cicoira, F.; Malliaras, G. G.; Park, J. Photoelectrical Imaging and Characterization of Point Contacts in Pentacene Thin-Film Transistors. *Appl. Phys. Lett.* **2010**, *97*, 023308.
13. Wang, S. D.; Minari, T.; Miyadera, T.; Tsukagoshi, K.; Aoyagi, Y. Contact-Metal Dependent Current Injection in Pentacene Thin Film Transistors. *Appl. Phys. Lett.* **2007**, *91*, 203508.
14. Saudari, S. R.; Frail, P. R.; Kagan, C. Ambipolar Transport in Solution-Deposited Pentacene Transistors Enhanced by Molecular Engineering of Device Contacts. *Appl. Phys. Lett.* **2009**, *95*, 023301.
15. Asadi, K.; Wu, Y.; Gholamrezaie, F.; Rudolf, P.; Blom, P. W. M. Single-Layer Pentacene Field-Effect Transistors Using Electrodes Modified with Self Assembled Monolayers. *Adv. Mater.* **2009**, *21*, 4109–4114.
16. Cheng, X.; Noh, Y. Y.; Wang, J.; Tello, M.; Frisch, J.; Blum, R. P.; Vollmer, A.; Rabe, J.; Koch, N.; Sirringhaus, H. Controlling Electron and Hole Injection in Ambipolar Organic Field-Effect Transistors by Self Assembled Monolayers. *Adv. Funct. Mater.* **2009**, *19*, 2407–2415.
17. Boudinet, D.; Benwadih, M.; Qi, Y.; Altazin, S.; Verillhac, J. M.; Kroger, M.; Serbutoviez, C.; Gwoziecki, R.; Coppard, R.; Le Blevennec, G.; *et al.* Modification of Gold Source and Drain Electrodes by Self-Assembled Monolayer in Staggered n- and p-Channel Organic Thin Film Transistors. *Org. Electron.* **2010**, *11*, 227–237.
18. Avouris, Ph.; Martel, R. Progress in Carbon Nanotube Electronics and Photonics. *MRS Bull.* **2010**, *35*, 306–313.
19. Heinze, S.; Tersoff, J.; Martel, R.; Derycke, V.; Appenzeller, J.; Avouris, Ph. Carbon Nanotubes as Schottky Barrier Transistors. *Phys. Rev. Lett.* **2002**, *89*, 106801.
20. Appenzeller, J.; Knoch, J.; Derycke, V.; Martel, R.; Wind, S.; Avouris, Ph. Field-Modulated Carrier Transport in Carbon Nanotube Transistors. *Phys. Rev. Lett.* **2002**, *89*, 126801.
21. Léonard, F.; Tersoff, J. Role of Fermi-Level Pinning in Nanotube Schottky Diodes. *Phys. Rev. Lett.* **2000**, *84*, 4693–4696.
22. Martel, R.; Derycke, V.; Lavoie, C.; Appenzeller, J.; Chan, K. K.; Tersoff, J.; Avouris, Ph. Ambipolar Electrical Transport in Semiconducting Single-Wall Carbon Nanotubes. *Phys. Rev. Lett.* **2001**, *87*, 256805.
23. Cao, Q.; Rogers, J. A. Ultrathin Films of Single-Walled Carbon Nanotubes for Electronics and Sensors: A Review of Fundamental and Applied Aspects. *Adv. Mater.* **2009**, *21*, 29–53.
24. Aguirre, C. M.; Ternon, C.; Paillet, M.; Desjardins, P.; Martel, R. Carbon Nanotubes as Injection Electrodes for Organic Thin Film Transistors. *Nano Lett.* **2009**, *9*, 1457–1461.
25. Aguirre, C. M.; Auvray, S.; Pigeon, S.; Izquierdo, R.; Desjardins, P.; Martel, R. Carbon Nanotube Sheets as Electrodes in Organic Light-Emitting Diodes. *Appl. Phys. Lett.* **2006**, *88*, 183104.
26. Qi, P.; Javey, A.; Rolandi, M.; Wang, Q.; Yenilmez, E.; Dai, H. Miniature Organic Transistors with Carbon Nanotubes as Quasi-One-Dimensional Electrodes. *J. Am. Chem. Soc.* **2004**, *126*, 11774–11775.

27. Cao, Y.; Steigerwald, M. L.; Nuckols, C.; Guo, X. Current Trends in Shrinking the Channel Length of Organic Transistor Down to the Nanoscale. *Adv. Mater.* **2010**, *22*, 20–32.
28. Cao, Q.; Zhu, Z. T.; Lemaitre, M. G.; Xia, M. G.; Shin, M.; Rogers, J. A. Transparent Flexible Organic Thin-Film Transistors that Use Printed Single-Walled Carbon Nanotube Electrodes. *Appl. Phys. Lett.* **2006**, *88*, 113511.
29. Yu, Z. B.; Hu, L. B.; Liu, Z. T.; Sun, M. L.; Wang, M. L.; Grüner, G.; Pei, Q. Fully Bendable Polymer Light Emitting Devices with Carbon Nanotubes as Cathode and Anode. *Appl. Phys. Lett.* **2009**, *95*, 203304.
30. Meijer, E. J.; Detcheverry, C.; Baesjou, P. J.; van Veenendaal, E.; de Leeuw, D. M.; Klapwijk, T. M. Dopant Density Determination in Disordered Organic Field Effect Transistors. *J. Appl. Phys.* **2003**, *93*, 4831–4135.
31. Santato, C.; Cicoira, F.; Cosseddu, P.; Bonfiglio, A.; Bellutti, P.; Muccini, M.; Zamboni, R.; Rosei, F.; Mantoux, A.; Doppelt, P. Organic Light-Emitting Transistors Using Concentric Source/Drain Electrodes on a Molecular Adhesion Layer. *Appl. Phys. Lett.* **2006**, *88*, 163511.
32. Anthopoulos, T. D.; Tanase, C.; Setayesh, S.; Meijer, E. J.; Hummelen, J. C; Blom, P. W. M.; de Leeuw, D. M. Ambipolar Organic Field-Effect Transistors Based on a Solution Processed Methanofullerene. *Adv. Mater.* **2004**, *16*, 2174–2179.
33. Singh, Th. B.; Marjanovic, N.; Stadler, P.; Auinger, M.; Matt, G. J.; Günes, S.; Sariciftci, N. S.; Schwödiauer, R.; Bauer, S. Fabrication and Characterization of Solution-Processed Methanofullerene-Based Organic Field-Effect Transistors. *J. Appl. Phys.* **2005**, *97*, 083714.
34. Tiwari, S. P.; Zhang, X. H.; Postcavage, W. J.; Kippelen, B. Study of Electrical Performance and Stability of Solution Processed n-Channel Organic Field-Effect Transistors. *J. Appl. Phys.* **2009**, *106*, 054504.
35. Cho, S.; Seo, J. H.; Lee, K.; Heeger, A. J. Enhanced Performance of Fullerene n-Channel Field-Effect Transistors with Titanium Sub-Oxide Injection Layer. *Adv. Funct. Mater.* **2009**, *19*, 1459–1464.
36. Seo, J. H.; Gutacker, A.; Walker, B.; Cho, S. N.; Garcia, A.; Yang, R. Q.; Nguyen, T. Q.; Heeeger, A. J.; Bazan, G. C. Improved Injection in n-Type Organic Transistors with Conjugated Polyelectrolyte. *J. Am. Chem. Soc.* **2009**, *131*, 18220–18221.
37. Thompson, B. C.; Frechet, J. M. Organic Photovoltaics-Polymer-Fullerene-Composite Solar Cell. *Angew. Chem., Int. Ed.* **2008**, *47*, 58–77.
38. Suzuki, S.; Watanabe, Y.; Homma, Y.; Fukuba, S.; Heun, S.; Locatelli, A. Work Functions of Individual Single-Wall Carbon Nanotubes. *Appl. Phys. Lett.* **2004**, *85*, 127–129.
39. Kroon, R.; Lenes, M.; Humelen, J. C.; Blom, P. W. M.; de Boer, B. Small Bandgap Polymers for Organic Solar Cells (Polymer Material Development in the Last 5 Years). *Polym. Rev.* **2008**, *48*, 531–582.
40. Meijer, E. J.; de Leeuw, D. M.; Setayesh, S.; Van Veenendaal, E.; Huisman, B. H.; Blom, P. W. M.; Hummelen, J. C.; Scherf, U.; Klapwijk, T. M. Solution-Processed Ambipolar Organic Field-Effect Transistors and Inverters. *Nat. Mater.* **2003**, *2*, 678–682.
41. Karl, N. Charge Carrier Transport in Organic Semiconductors. *Synth. Met.* **2003**, *133*, 649–657.
42. Blanchet, G. B.; Fincher, C. R.; Lefenfeld, M.; Rogers, J. A. Contact Resistance in Organic Thin Film Transistors. *Appl. Phys. Lett.* **2004**, *84*, 296–298.
43. Methods to extract the contact resistance in OTFTs with nonlinear I_d/V_d relationship have been described in refs 7 and 9. However, evaluation of contact resistance of Au OTFTs presented here is beyond the scope of this paper and not necessary because the difference between CNT and Au OTFTs is evident.
44. von Hauff, E.; Parisi, J.; Dyakonov, V. Investigation of Electron Injection in a Methanofullerene Thin Film Transistor. *J. Appl. Phys.* **2006**, *100*, 073713.
45. Meijer, E. J.; Gelinck, G. H.; van Veenendaal, E.; Huisman, B. H.; de Leeuw, D. M.; Klapwijk, T. M. Scaling Behavior and Parasitic Series Resistance in Disordered Organic Field-Effect Transistors. *Appl. Phys. Lett.* **2003**, *82*, 4576–4578.
46. Molinari, A.; Gutierrez, I.; Holea, I. N.; Russo, S.; Morpurgo, A. F. Bias-Dependent Contact Resistance in Rubrene Single-Crystal Field-Effect Transistors. *Appl. Phys. Lett.* **2007**, *90*, 212103.
47. For Au OTFTs, SS is significantly higher (although hard to extract because I_d does not depend exponentially on V_g in the subthreshold region).
48. Sze, S.M. *Physics of Semiconducting Devices*; Wiley: New York, 1981.
49. Salleo, A.; Endicott, F.; Street, R. A. Reversible and Irreversible Trapping at Room Temperature in Poly(thiophene) Thin-Film Transistors. *Appl. Phys. Lett.* **2005**, *86*, 263505.
50. Mathijssen, S. G. J.; Kemerink, M.; Sharma, A.; Colle, M.; Bobbert, P. A.; Jansssen, R. A. J.; de Leeuw, D. M. Charge Trapping at the Dielectric of Organic Transistors Visualized in Real Time and Space. *Adv. Mater.* **2008**, *20*, 975–979.
51. Kaji, T.; Entani, S.; Ikeda, S.; Saiki, K. Origin of Carrier Types in Intrinsic Organic Semiconductors. *Adv. Mater.* **2008**, *20*, 2084–2089.
52. de Boer, R. W. I.; Stassen, A. F.; Craciun, M. F.; Mulder, C. L.; Molinari, A.; Rogge, S.; Morpurgo, A. F. Ambipolar Cu- and Fe-Phthalocyanine Single-Crystal Field-Effect Transistors. *Appl. Phys. Lett.* **2005**, *86*, 262109.
53. Appenzeller, J.; Knoch, J.; Martel, R.; Derycke, V.; Wind, S. J.; Avouris, Ph. Carbon Nanotube Electronics. *IEEE Trans. Nanotechnol.* **2002**, *1*, 184–189.
54. Aguirre, C. M.; Levesque, P. L.; Paillet, M.; Lapointe, F.; St-Antoine, B. C.; Desjardins, P.; Martel, R. The Role of the Oxygen/Water Redox Couple in Suppressing Electron Conduction in Field Effect Transistors. *Adv. Mater.* **2009**, *21*, 3087–3091.
55. Zhao, Q. T.; Kluth, P.; Winnerl, S.; Mantl, S. Fabrication of Schottky Barrier MOSFETs on SOI by a Self-Assembled $CoSi_2$-Patterning Method. *Solid-State Electron.* **2003**, *47*, 1183–1186.
56. Osikowicz, W.; de Jong, M. P.; Braun, S.; Tengstedt, C.; Fahlman, M.; Salaneck, W. R. Energetics at Au Top and Bottom Contacts on Conjugated Polymers. *Appl. Phys. Lett.* **2006**, *88*, 193504.
57. Larson, J. M. Overview and Status of Metal S/D Schottky-Barrier MOSFET Technology. *IEEE Trans. Electron. Dev.* **2006**, *53*, 1048–1058.
58. In carbon nanotube field-effect transistors, charges are injected from a metallic electrode into a 1D CNT semiconductor, whereas in our CNT OTFTs, charges are injected from a 1D CNT electrode into an organic semiconductor. In both cases, 1D electrostatics describe best the situation because of the form factor of CNTs.
59. Luo, J. T.; Wu, W. F.; Wen, H. C.; Wan, B. Z.; Chang, Y. M.; Chou, C. P.; Chen, J. M.; Chen, W. N. The Role of Hydrophobic Groups on the Surface of Ultra Low Dielectric Constant Porous Silica Film During Thermal Treatment. *Thin Solid Films* **2007**, *515*, 7275–7280.